Nonlinear Analysis of Magnetic Gear Dynamics Using Superposition and Conservation of Energy

Matthew C. Gardner
Dept. Elec. & Comp. Engineering.
Texas A&M University
College Station, TX, USA
gardner1100@tamu.edu

Hamid A. Toliyat
Dept. Elec. & Comp. Engineering.
Texas A&M University
College Station, TX, USA
toliyat@tamu.edu

Abstract—**This paper presents an analytical approach to the nonlinear dynamics of magnetic gears. Without compromising the system's nonlinearity, a magnetic gear's motion can be separated into rigid body motion and motion about a fixed center. Then, neglecting losses, the behavior of the torque angle can be evaluated using the conservation of energy principle. This approach shows excellent agreement with a Simulink model and a transient finite element analysis (FEA) model of a magnetic gear with sinusoidal torque angle curves. However, there are some discrepancies in the predicted velocities and oscillation frequencies compared to results produced by FEA models of designs with significant torque ripples, but the proposed approach still agrees with each of the FEA models about whether the gear will slip for over 98.5% of the cases. Also, cases with viscous friction are considered, but this has a limited effect on the system's dynamic behavior immediately after a change in the applied torques. With viscous friction, the proposed approach still agrees with each of the FEA models about whether the gear will slip for at least 93.5% of the cases. This analysis also demonstrates the significant impact of the effective inertia ratio on the system's dynamic performance.**

Keywords—control, dynamics, gear ratio, inertia, magnetic gear, nonlinear, oscillation, slip, superposition, torque angle, torque ripple

I. INTRODUCTION

Like mechanical gears, magnetic gears convert mechanical power between high-speed, low-torque rotation and low-speed, high-torque rotation. However, instead of transferring power through mechanically interlocking teeth, magnetic gears employ interacting magnetic fields. This noncontact operation affords magnetic gears many potential advantages, such as inherent overload protection, improved reliability, reduced maintenance, and physical isolation between shafts. Thus, magnetic gears have attracted significant research interest [1]-[15] and have been proposed for a wide range of applications, including wind turbines [4], wave energy generation [5]-[6], ship propulsion [7], electric vehicles [8], and aerospace applications [9].

The noncontact nature of magnetic gearing also introduces some challenges. First, if torque is applied too suddenly or if too much is applied, the magnetic gear can slip, decoupling the rotation of the two shafts. While slipping is often better than the permanent damage that can occur if too much torque is applied to a mechanical gear, it is still desirable to avoid slipping when possible. Second, the magnetic coupling between the two rotors is not as stiff as the coupling in a mechanical gear. This can result in a quite underdamped system, especially if the magnetic gear is very efficient [10]-[12]. Third, the torque on both rotors

is a nonlinear function of their positions [10]-[13]. Many papers on the dynamics or control of magnetic gears linearize the system around an operating point [10], [12]. However, this is inaccurate when there is a significant change in torques [13]. Other papers employ numerical time-stepping models to accurately model the nonlinearity [11], but this provides less intuition and insight into the dynamic behavior of magnetic gears. This paper provides a nonlinear analytical model for the dynamic behavior of magnetically geared systems and presents relevant insights into parameters affecting this behavior.

II. MAGNETIC GEAR DYNAMIC MODEL

As in [10], [12]-[13], a magnetic gear can be dynamically modeled as two inertias separated by two ideal gearboxes and a nonlinear torsional spring, as shown in Fig. 1 and described by

$$J_h \frac{d\omega_h}{dt} = T_M - B_h\omega_h - p_h T_C \sin(p_h\theta_h - p_l\theta_l) \qquad (1)$$

$$J_l \frac{d\omega_l}{dt} = T_L - B_l\omega_l + p_l T_C \sin(p_h\theta_h - p_l\theta_l), \qquad (2)$$

where J_h, ω_h, B_h, p_h, and θ_h are the moment of inertia, angular velocity, viscous friction coefficient, pole pair count, and angular position of the high speed side, J_l, ω_l, B_l, p_l, and θ_l are the same quantities for the low speed side, T_M is the torque provided by the machine connected to the high speed rotor (HSR), T_L is the torque of the load connected to the low speed rotor (LSR), and T_C is the gear's characteristic torque, which is defined as the slip torque on either rotor divided by the number of pole pairs on that rotor. The torque angle, θ_T, is defined as

$$\theta_T = p_h\theta_h - p_l\theta_l. \qquad (3)$$

These equations can describe several different types of magnetic gears, including coaxial, spur, and cycloidal topologies, with the appropriate choices of p_h and p_l, which should result in a gear ratio, $G = \frac{p_l}{p_h}$. One of the pole pair counts may be the number of modulators for a coaxial gear [3], [4] or simply 1 in the case of a cycloidal gear [2]. Additionally, in cases where the rotors rotate in opposite directions, p_h or p_l should be negative [1]-[3].
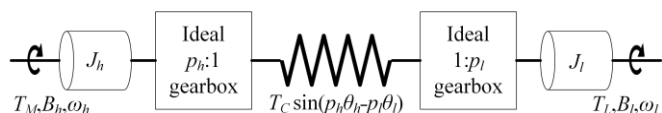

Fig. 1. Magnetic gear dynamic model.

As in [14], the system can be transformed by referring the HSR and LSR quantities through the ideal gearboxes. This produces the model illustrated in Fig. 2 and described by

$$J_h' \frac{d\omega_h'}{dt} = T_M' - B_h'\omega_h' - T_C \sin(\theta_h' - \theta_l') \quad (4)$$

$$J_l' \frac{d\omega_l'}{dt} = T_L' - B_l'\omega_l' + T_C \sin(\theta_h' - \theta_l'), \quad (5)$$

where $J_h' = \frac{J_h}{p_h^2}$, $T_M' = \frac{T_M}{p_h}$, $B_h' = \frac{B_h}{p_h^2}$, $\omega_h' = \omega_h p_h$, $\theta_h' = \theta_h p_h$, $J_l' = \frac{J_l}{p_l^2}$, $T_L' = \frac{T_L}{p_l}$, $B_l' = \frac{B_l}{p_l^2}$, $\omega_l' = \omega_l p_l$, and $\theta_l' = \theta_l p_l$. This model is effectively analogous to a magnetic coupling or a magnetic gear with a 1:1 gear ratio.
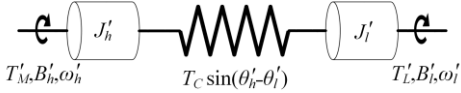
Fig. 2.   Magnetic gear dynamic model transformed to 1:1 gear ratio.

A. *Superposition of Rigid Body and Fixed Center Motions*

It is assumed that the viscous friction on each rotor is proportional to its inertia, $\frac{B_h'}{J_h'} = \frac{B_l'}{J_l'}$, (or that the design is relatively efficient and the friction on each rotor can be neglected). Then, using superposition, the motion of the gear can be decomposed into the sum of the motions of the two systems shown in Fig. 3, with the torques given by

$$T_h^{RB} = \frac{(T_M' + T_L')J_h'}{J_h' + J_l'} \quad (6)$$

$$T_l^{RB} = \frac{(T_M' + T_L')J_l'}{J_h' + J_l'} \quad (7)$$

$$T^{FC} = \frac{T_M'J_l' - T_L'J_h'}{J_h' + J_l'}. \quad (8)$$

This superposition satisfies the following conditions: $T_M' = T_h^{RB} + T^{FC}$, $T_L' = T_l^{RB} - T^{FC}$, $\omega_h' = \omega^{RB} + \omega_h^{FC}$, $\omega_l' = \omega^{RB} - \omega_l^{FC}$, $\theta_h' = \theta^{RB} + \theta_h^{FC}$, and $\theta_l' = \theta^{RB} - \theta_l^{FC}$.
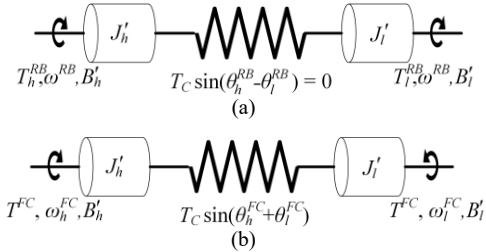

(a)

(b)

Fig. 3.   The motion of the magnetic gear can be expressed as the superposition of (a) rigid body motion and (b) changes in the torque angle. Note that the positive direction of rotation on the LSR is different between (a) and (b).

Since both rotors in Fig. 3(a) have the same acceleration, $\alpha^{RB} = \frac{T_h^{RB} - B_h'\omega^{RB}}{J_h'} = \frac{T_l^{RB} - B_l'\omega^{RB}}{J_l'}$, and the initial conditions presume that both rotors in Fig. 3(a) have the same initial speeds and angles, both inertias in Fig. 3(a) always have the same

speeds and angles as each other. Thus, the rigid body torque angle, $\theta_h^{RB} - \theta_l^{RB}$, is always zero, and the nonlinear spring torque in Fig. 3(a) is always zero. Since this rigid body motion does not affect the system's torque angle, superposition can isolate the rigid body motion of Fig. 3(a) from the torque angle changes in Fig. 3(b) without violating the system's nonlinearity.

Since equal and opposite torques are applied to the two shafts in Fig. 3(b), the net torque is always zero. Thus, the system can be represented as the motion of each rotor relative to a fixed point, as shown in Fig. 4(a). This is analogous to the fixed center of mass in a system with zero net force. As the same torque is applied to J_h' and J_l', their accelerations, α_h^{FC} and α_l^{FC}, are inversely proportional to their respective inertias, such that $\frac{\alpha_h^{FC}}{\alpha_l^{FC}} = \frac{J_l'}{J_h'}$. Thus, with the condition that $\frac{\omega_h^{FC}}{\omega_l^{FC}} = \frac{\theta_h^{FC}}{\theta_l^{FC}} = \frac{J_l'}{J_h'}$ at the initial time, these initial equalities hold true at all times, so each side of Fig. 4(a) can be transformed to the torque angle reference frame in Fig. 4(b) with $\theta_T = \theta_h^{FC} \cdot \left(1 + \frac{J_h'}{J_l'}\right) = \theta_l^{FC} \cdot \left(1 + \frac{J_l'}{J_h'}\right)$, $\omega_T = \omega_h^{FC} \cdot \left(1 + \frac{J_h'}{J_l'}\right) = \omega_l^{FC} \cdot \left(1 + \frac{J_l'}{J_h'}\right)$, $J_T = \frac{J_h'J_l'}{J_h' + J_l'}$, and $B_T = \frac{B_h'B_l'}{B_h' + B_l'}$. Thus, the behavior of the torque angle, which is critical to the analysis of both slipping and the gear's oscillations, can be evaluated in terms of the dynamics of a single inertia connected to a fixed point by a nonlinear spring.
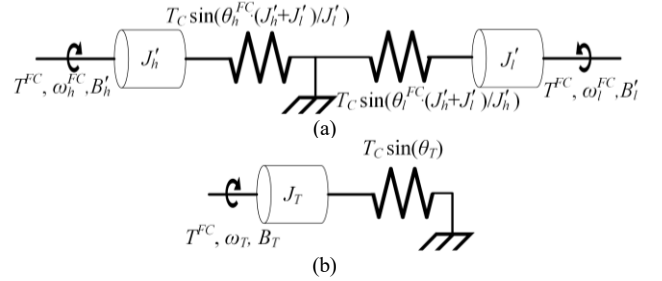

(a)

(b)

Fig. 4.   Both the HSR and the LSR (a) represented as moving relative to a fixed center of inertia and (b) transformed to the torque angle reference frame.

B. *Conservation of Energy*

This system could be evaluated by linearizing the spring about an operating point and solving in the frequency domain, but, if the losses are assumed to be negligible, the conservation of energy principle yields an approach that preserves the nonlinearity. For the torque angle reference frame of Fig. 4(b), energy enters or leaves the system as T^{FC} is applied and the inertia rotates. Energy is also converted between the rotational kinetic energy of the inertia and the potential energy of the spring. If T^{FC} is known as a function of the torque angle, the kinetic energy can be determined as a function of the torque angle. Fig. 5 illustrates this for the case where the gear is initially in steady-state at a torque angle of θ_T^i, and T^{FC} suddenly increases. In Fig. 5, the rotational kinetic energy at a torque angle of θ can be found by subtracting the area under the nonlinear torque curve (the spring's potential energy) from the area under the step torque curve (the input energy). This can be used to calculate the angular velocity of the rotating inertia in Fig. 4(b) at any torque angle. The system will oscillate as energy from the external torque enters or leaves the system and is transformed between potential energy and kinetic energy. Any

losses in the system will dissipate the energy, and, if it does not slip, it will eventually reach steady-state at the torque angle where the nonlinear spring's torque equals T^{FC}.
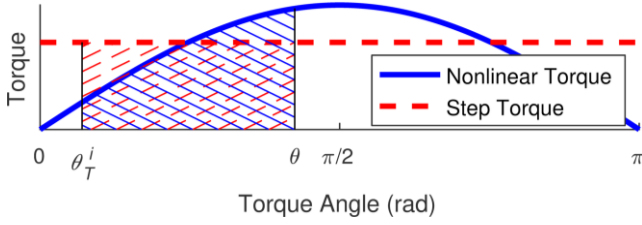

Fig. 5. The energy input into the Fig. 4(b) system is the area under the step torque curve, and the energy stored in the nonlinear spring is the area under the nonlinear torque curve. The kinetic energy of the inertia is the difference between these two energies (assuming negligible losses).

III. DESIGN IMPLICATIONS

A. Effective Inertia Ratio

Fig. 3(b) and (8) illustrate that the ratio between J_h' and J_l' directly determines the extent to which the torques on the two sides impact the torque angle. To quantify these trends, the effective inertia ratio, R_J, is defined as

$$R_J = \frac{J_l}{J_h G^2} = \frac{J_l'}{J_h'}. \tag{9}$$

If the machine and the physical load are stiffly connected to the HSR and LSR, respectively, then, J_h and J_l should include their respective inertias, in addition to the inertias of the gear's rotors. Fig. 6 shows what portions of the per unit external torques contribute to the changes in the torque angle for a given effective inertia ratio. Thus, R_J significantly affects the system's dynamic performance. A large R_J means that disturbances in the load torque will have less effect on the torque angle, which is advantageous if the load torque may change suddenly, but disturbances in the machine torque will cause larger torque angle oscillations. Additionally, with a large R_J, a transient load torque much larger than the LSR slip torque may not necessarily cause the gear to slip, if it is not opposed by a corresponding torque from the machine. Alternatively, a small R_J will make the gear's oscillatory and slipping behavior more susceptible to the load torque and less susceptible to the machine torque, which could be advantageous if the machine has a high torque ripple and the load changes relatively slowly. Furthermore, R_J determines how much of the oscillations appear in θ_h^{FC} and θ_l^{FC}. Increasing R_J will increase the extent of oscillations on the HSR while reducing the extent of oscillations on the LSR. Thus, when selecting the gear ratio, the designer must consider both the gear ratio's impact on the overall size of the system [6], [15] and its impact on the system's dynamic behavior.
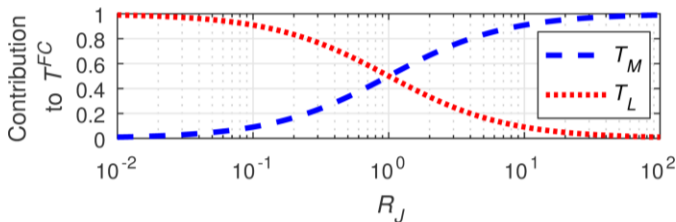

Fig. 6. The impact of R_J on how much the per unit (relative to the slip torques of their respective rotors) machine torque and load torque contribute to T^{FC}.

B. Responses to Step Changes in Torque

The conservation of energy approach has two significant limitations. First, the torques must be known as a function of position, rather than time, and, second, it assumes that the losses are negligible. However, this approach can still address one significant issue: whether a given step change in torque on either side of the gear will cause it to slip. With a step change in torque, the torque is known with respect to position. Also, magnetic gears are often quite underdamped, so very little energy is lost by the time the gear reaches the maximum extent of its torque angle oscillation for the first time after the step change [10], [11]. The maximum torque angle reached, θ_T^m, is the angle at which the kinetic energy of the rotating inertia reaches 0, which is where the energy input into the Fig. 4(b) system equals the change in the energy stored in the nonlinear spring, as given by

$$\int_{\theta_T^i}^{\theta_T^m} T^{FC} d\theta_T = \int_{\theta_T^i}^{\theta_T^m} T_C \sin(\theta_T)\, d\theta_T, \tag{10}$$

where the torque angle was initially in steady-state at θ_T^i. In the case of a step change in torque, (10) becomes

$$T^{FC} \cdot \left(\theta_T^m - \theta_T^i\right) = T_C \cdot \left(\cos\left(\theta_T^i\right) - \cos\left(\theta_T^m\right)\right), \tag{11}$$

where T^{FC} is the torque in Fig. 4(b) after the step change. This is equivalent to finding the angle where the areas under the step torque and the nonlinear torque curves in Fig. 5 are equal. The trivial solution, $\theta_T^m = \theta_T^i$, is the minimum boundary of the oscillation, which is the initial torque angle. The nontrivial solution of (11) gives the maximum boundary of the oscillation. If no nontrivial solution exists, the gear will slip. To check this, the kinetic energy can be evaluated at the torque angle between $\pi/2$ and π where T^{FC} is equal to the nonlinear spring torque, $\theta_T^{slip} = \pi - \sin^{-1}\left(\frac{T^{FC}}{T_C}\right)$. For the gear not to slip, T^{FC} must be less than T_C, and the following condition must also be true:

$$\left(\theta_T^{slip} - \theta_T^i\right) < \frac{T_C}{T^{FC}} \cdot \left(\cos\left(\theta_T^i\right) - \cos\left(\theta_T^{slip}\right)\right). \tag{12}$$

The angular velocity of the inertia in the torque angle reference frame can be determined as a function of the torque angle from the inertia's kinetic energy:

$$\omega_T(\theta_T) = \pm\sqrt{\frac{2}{J_T} \int_{\theta_T^i}^{\theta_T} (T^{FC} - T_C \sin(\theta))d\theta}, \tag{13}$$

assuming that losses are negligible. The angular velocity in the torque angle reference frame can be transformed back to the Fig. 1 model to determine the angular velocities of the oscillations on each rotor. If the step change in torque does not cause the gear to slip, the maximum angular velocity in the torque angle reference frame, ω_T^{max}, occurs at the torque angle between 0 and $\pi/2$ where the torque from the nonlinear spring is equal to T^{FC}, $\theta_T^{eq} = \sin^{-1}\left(\frac{T^{FC}}{T_C}\right)$, and can be calculated as

$$\omega_T^{max} = \sqrt{\frac{2 \cdot \left(T^{FC} \cdot (\theta_T^{eq} - \theta_T^i) - T_C \cdot (\cos(\theta_T^i) - \cos(\theta_T^{eq}))\right)}{J_T}}. \tag{14}$$

With the velocity known as a function of the torque angle, the frequency of oscillation can be calculated as

$$f_o = \left(2 \int_{\theta_T^i}^{\theta_T^m} \frac{1}{\omega_T(\theta_T)} d\theta_T \right)^{-1}, \qquad (15)$$

using the positive sign in (13). Similar equations can be derived for cases where changing T^{FC} decreases the torque angle.
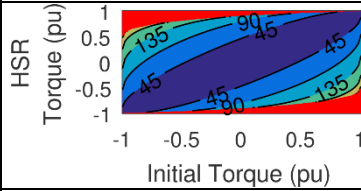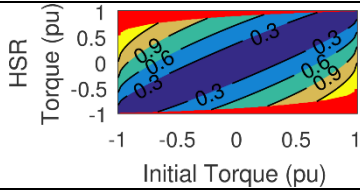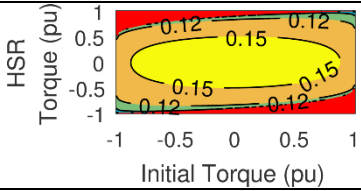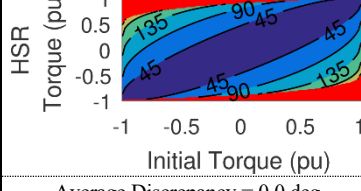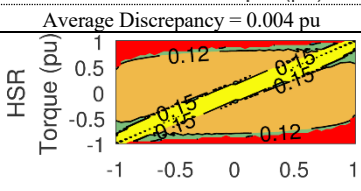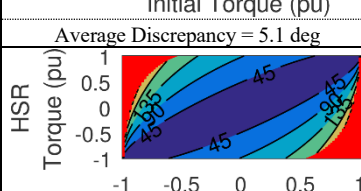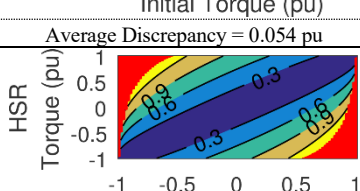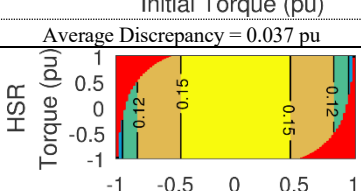
IV. MODEL VALIDATION
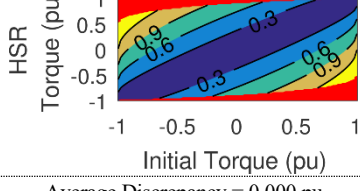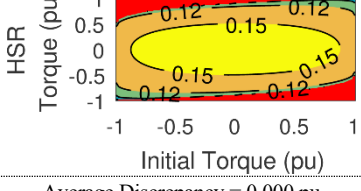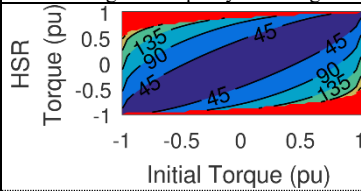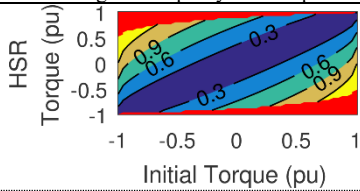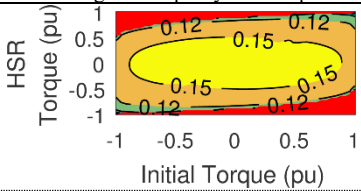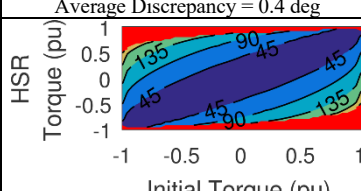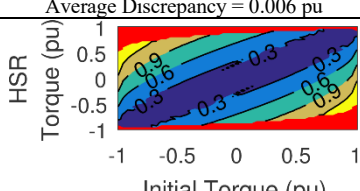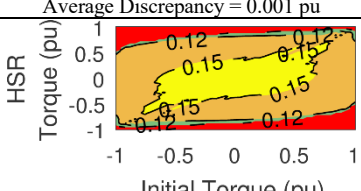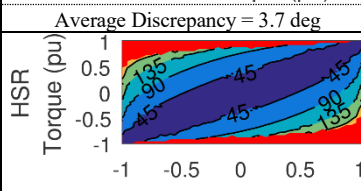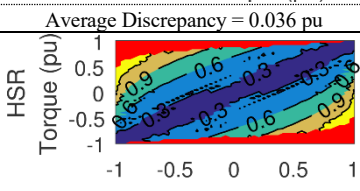
Tables I – IV compare several different analysis methods to determine the accuracy of the proposed model. The proposed nonlinear model is used to evaluate a scenario where the external torque applied to the HSR is suddenly changed to various per unit values starting from different initial steady-state torque angles. The external torque on the LSR is kept at its initial value. The magnitude of the torque angle oscillation, the maximum angular velocity of the inertia in the torque angle reference frame, and the oscillation frequency are calculated using (11), (14), and (15), respectively. Two values of R_J are considered. In each case, J_T is set to 1 pu where, in the torque angle reference frame, the base torque, time, and angle are T_C, 1 s, and 1 rad, respectively. The base torque for each rotor is the slip torque of that rotor. The results are compared against those produced by a Simulink model with the same parameters, which is shown in Fig. 7. The proposed model and the Simulink model assume that

TABLE I.   ANALYSIS METHODS COMPARISON WITH $R_J = 0.25$ AND $B_T = 0$ PU

Model	Slip Prediction Agreement	Torque Angle Oscillation (deg)	Maximum Angular Velocity (pu)	Oscillation Frequency (pu)
Proposed	N/A	*(contour plot: HSR Torque (pu) vs Initial Torque (pu))*	*(contour plot)*	*(contour plot)*
Simulink	100.0%	*(contour plot)* Average Discrepancy = 0.0 deg	*(contour plot)* Average Discrepancy = 0.000 pu	*(contour plot)* Average Discrepancy = 0.000 pu
FEA 1	99.7%	*(contour plot)* Average Discrepancy = 0.5 deg	*(contour plot)* Average Discrepancy = 0.004 pu	*(contour plot)* Average Discrepancy = 0.000 pu
FEA 2	98.8%	*(contour plot)* Average Discrepancy = 4.0 deg	*(contour plot)* Average Discrepancy = 0.024 pu	*(contour plot)* Average Discrepancy = 0.008 pu
FEA 3	98.7%	*(contour plot)* Average Discrepancy = 4.4 deg	*(contour plot)* Average Discrepancy = 0.032 pu	*(contour plot)* Average Discrepancy = 0.010 pu
Linearized	85.3%	*(contour plot)* Average Discrepancy = 12.4 deg	*(contour plot)* Average Discrepancy = 0.032 pu	*(contour plot)* Average Discrepancy = 0.015 pu

TABLE II. ANALYSIS METHODS COMPARISON WITH $R_J = 4$ AND $B_T = 0$ PU

Model	Slip Prediction Agreement	Torque Angle Oscillation (deg)	Maximum Angular Velocity (pu)	Oscillation Frequency (pu)
Proposed	N/A			
Simulink	100.0%			
		Average Discrepancy = 0.0 deg	Average Discrepancy = 0.000 pu	Average Discrepancy = 0.000 pu
FEA 1	100.0%			
		Average Discrepancy = 0.4 deg	Average Discrepancy = 0.006 pu	Average Discrepancy = 0.001 pu
FEA 2	98.8%			
		Average Discrepancy = 3.7 deg	Average Discrepancy = 0.036 pu	Average Discrepancy = 0.004 pu
FEA 3	98.6%			
		Average Discrepancy = 5.1 deg	Average Discrepancy = 0.054 pu	Average Discrepancy = 0.037 pu
Linearized	86.6%			
		Average Discrepancy = 12.4 deg	Average Discrepancy = 0.032 pu	Average Discrepancy = 0.015 pu

the torque is a sinusoidal function of the torque angle, but, in an actual magnetic gear, harmonics produce torque ripples on the rotors. Thus, transient finite element analysis (FEA) is used to evaluate three coaxial gear designs, FEA 1, FEA 2, and FEA 3, with gear ratios of -2.053:1, -12.33:1, and -12:1, respectively, which are depicted in Fig. 8. Fig. 9 shows the torque angle curves of these designs. FEA 1's torque angle curves are very sinusoidal due to the high least common multiple of the pole counts [4]. However, due to its integer gear ratio, FEA 3's HSR torque angle curve is more distorted. FEA 2's torque angle curve is more distorted than that of FEA 1 but less distorted than that of FEA 3. For the FEA, eddy effects in the NdFeB N42 magnets and core losses in the M47 modulators and back irons

also affect the torques on the two rotors. In each case, both rotors are assumed to be initially stationary. A model linearized about the initial torque angle is also used to evaluate the designs.
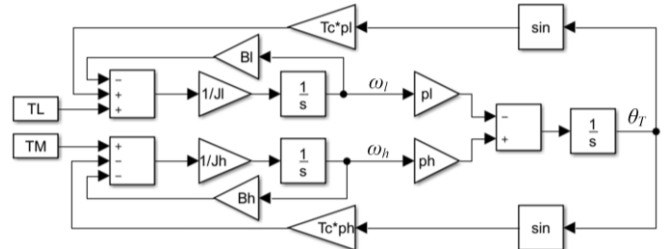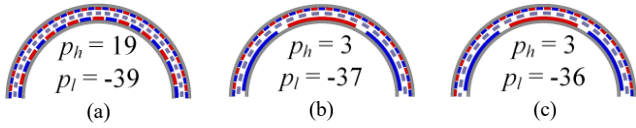

Fig. 7. The Simulink model used in this study.

$p_h = 19$
$p_l = -39$
(a)

$p_h = 3$
$p_l = -37$
(b)

$p_h = 3$
$p_l = -36$
(c)

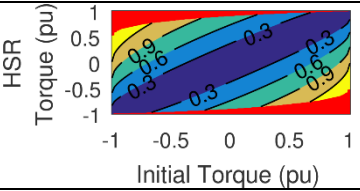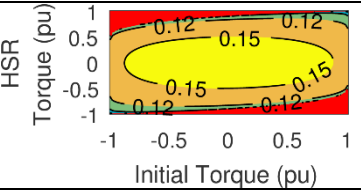Fig. 8.   (a) FEA 1, (b) FEA 2, and (c) FEA 3 coaxial magnetic gear designs.

(a)

(b)

(c)

— HSR
····· LSR
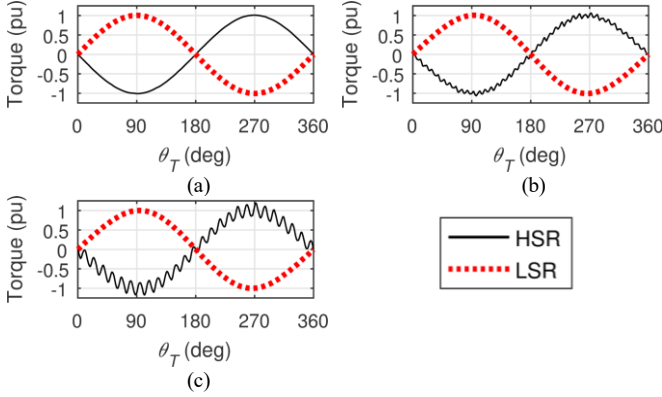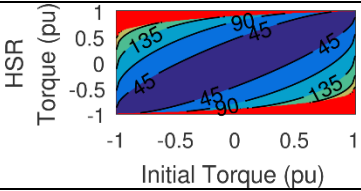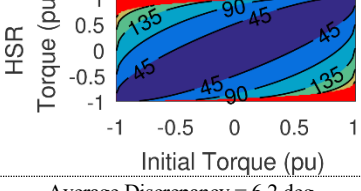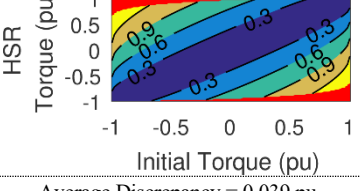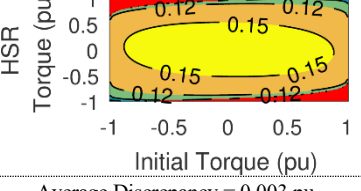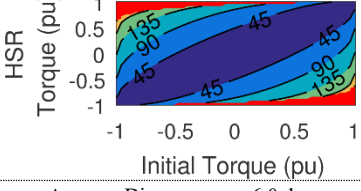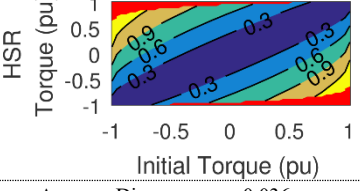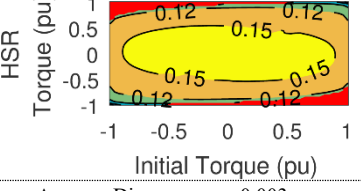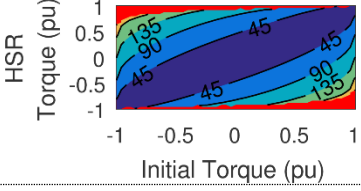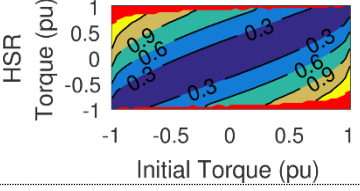
Fig. 9.   Torque angle curves of (a) FEA 1, (b) FEA 2, and (c) FEA 3.

Table I compares the results for each of the different analysis methods with $R_J = 0.25$, and Table II compares the results with $R_J = 4$. In Tables I and II, the red areas indicate cases that cause the gear to slip. Tables I and II also show the percentages of the cases in which the proposed model agrees with each of the other models about whether the gear will slip. For the cases that both models agree will not slip, Tables I and II provide the average value of the absolute difference between the quantities predicted by the two models. For the linearized model, the gear is assumed to slip if it reach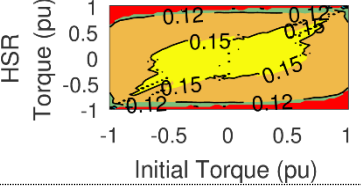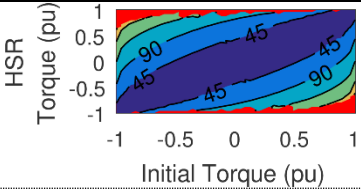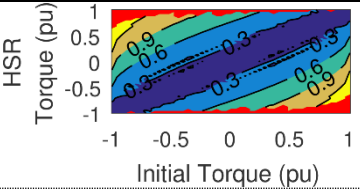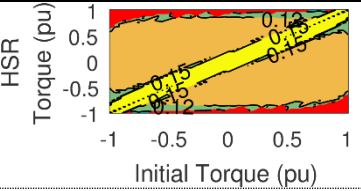es the same torque angle as would cause slipping in the nonlinear model ($\pi - \sin^{-1}(T^{FC}/T_C)$). The proposed model agrees very well with the Simulink model and with the FEA 1 model. However, for the FEA 2 and FEA 3 models, the torque ripple in the torque angle curves produces some discrepancies in the oscillation frequency and maximum angular velocity in the torque angle reference frame, especially when the applied torque does not change very much and the behavior of the system is dominated by the torque ripple, rather than the change in applied torque. The linearized model correlates well with the Simulink model and FEA 1 when the change in applied

TABLE III.   ANALYSIS METHODS COMPARISON WITH $R_J = 0.25$ AND $B_T = 0.1$ PU

Model	Slip Prediction Agreement	Torque Angle Oscillation (deg)	Maximum Angular Velocity (pu)	Oscillation Frequency (pu)
Proposed	N/A			
Simulink	95.9%	Average Discrepancy = 6.3 deg	Average Discrepancy = 0.039 pu	Average Discrepancy = 0.003 pu
FEA 1	95.6%	Average Discrepancy = 6.3 deg	Average Discrepancy = 0.039 pu	Average Discrepancy = 0.003 pu
FEA 2	96.5%	Average Discrepancy = 6.1 deg	Average Discrepancy = 0.052 pu	Average Discrepancy = 0.007 pu
FEA 3	96.5%	Average Discrepancy = 6.4 deg	Average Discrepancy = 0.055 pu	Average Discrepancy = 0.010 pu

TABLE IV.   ANALYSIS METHODS COMPARISON WITH $R_J = 4$ AND $B_T = 0.1$ PU

Model	Slip Prediction Agreement	Torque Angle Oscillation (deg)	Maximum Angular Velocity (pu)	Oscillation Frequency (pu)
Proposed	N/A			
Simulink	93.6%	Average Discrepancy = 6.2 deg	Average Discrepancy = 0.039 pu	Average Discrepancy = 0.003 pu
FEA 1	93.5%	Average Discrepancy = 6.0 deg	Average Discrepancy = 0.036 pu	Average Discrepancy = 0.003 pu
FEA 2	94.5%	Average Discrepancy = 6.0 deg	Average Discrepancy = 0.053 pu	Average Discrepancy = 0.005 pu
FEA 3	93.7%	Average Discrepancy = 6.9 deg	Average Discrepancy = 0.063 pu	Average Discrepancy = 0.037 pu

torque is small. However, the linearized model becomes quite inaccurate for larges changes in applied torque and incorrectly predicts whether the gear will slip for over 10% of the cases.

Tables I and II illustrate that with small R_J values, much larger torques can be applied to the HSR without slipping the gear. If the gear is driven by a motor on the HSR, this would allow the motor to rapidly accelerate the gear by applying torques larger than the HSR slip torque while the gear is accelerating. Tables I and II also illustrate that the oscillation frequency depends on both the starting torque angle and the change in applied torque. Because the nonlinear spring is stiffest at a torque angle of 0, the oscillation frequency is highest when the torque angle oscillates near 0, but the oscillation frequency becomes lower when the gear is close to slipping. However, for designs with large torque ripples, such as FEA 2 and FEA 3, the torque ripple significantly affects the oscillation frequency if the change in applied torque is small.

In Tables I and II, the FEA models incorporate the effects of eddy currents and core losses, but viscous friction is neglected in all cases. To illustrate the impact of B_T on the proposed model's accuracy, Tables III and IV compare the proposed model, which assumes the losses are negligible, against the Simulink and FEA models with $B_T = 0.1$ pu. Eddy current losses and core losses are again included in the FEA models.

Tables III and IV show that the viscous friction does prevent a few cases from slipping. Thus, the proposed model predicts that some cases would slip where the other models predict that those cases would not slip. Nonetheless, the proposed model still agrees with the each of the other models for at least 93.5% of the cases. Thus, even with B_T as high as 0.1 pu, the viscous friction has a limited impact on the transient performance of the system immediately after the change in applied torque. Even though the proposed model neglects the viscous friction, it can still predict the dynamic response of the system for the first torque angle oscillation after a step change in applied torque with reasonable accuracy. After this first oscillation, the viscous friction will gradually damp out the energy in the later oscillations. Therefore, if this first oscillation does not cause the gear to slip, the later oscillations will not cause it to slip, unless there is another change in the applied torque.

V. Conclusion

This paper presents a nonlinear approach for evaluating the dynamics of magnetic gears. First, superposition is applied to separate the rigid body motion of the two rotors from the motion about a fixed center. Second, this motion about a fixed center is transformed into the torque angle reference frame, which contains a single inertia and a single nonlinear torsional spring. Third, the extent of the torque angle oscillations, the maximum angular velocity, and the oscillation frequency are evaluated in the torque angle reference frame using the conservation of energy principle for the system (assuming losses are negligible). This approach is verified through comparison with Simulink and FEA results. The proposed model agrees extremely well with the Simulink model and a FEA model with very little torque ripple. However, for the FEA models with larger torque ripples, there are discrepancies between the velocities and oscillation frequencies predicted by the proposed approach and those predicted by the FEA when the system experiences only a small change in torque. These discrepancies result from the deviation from the assumed perfectly sinusoidal torque angle curves, so the only way to eliminate these discrepancies is to include the torque ripple in the model. Nonetheless, the proposed model agrees with each FEA model about whether the gear will slip for over 98.5% of the cases, and the proposed model is able to analyze cases significantly faster than FEA. On the other hand, a linearized model is shown to be inaccurate when there is a significant change in the torque applied to the gear. Thus, the linearized model incorrectly predicts whether the gear will slip for over 10% of the cases. A case with viscous friction is also evaluated using Simulink and FEA, but the viscous friction in this case makes a limited impact on the dynamic behavior of the system immediately following a change in the applied torque. Even though the proposed model does not consider losses, it still agrees with each FEA model for at least 93.5% of the cases when the FEA model considers viscous friction.

This analysis also reveals that the effective inertia ratio, which depends on the gear ratio and the inertias of the two rotors, has a significant impact on the dynamic performance of the system. It determines the extent to which torques applied to each rotor affect the torque angle of the gear and the extent to which oscillations of the torque angle cause oscillations on each rotor. A small effective inertia ratio means that the torques applied to the LSR will affect the torque angle much more than torques applied to the HSR and that torque angle oscillations will cause more oscillations on the LSR than on the HSR, whereas a large effective inertia ratio will have the opposite effects.

Acknowledgment

References

[1] K. Atallah and D. Howe, "A novel high-performance magnetic gear," *IEEE Trans. Magn.*, vol. 37, no. 4, pp. 2844–2846, Jul. 2001.

[2] F. T. Jorgensen, T. O. Andersen and P. O. Rasmussen, "The Cycloid Permanent Magnetic Gear," *IEEE Trans. Ind. Appl.*, vol. 44, no. 6, pp. 1659-1665, Nov./Dec. 2008.

[3] P. M. Tlali, R.-J. Wang, and S. Gerber, "Magnetic gear technologies: A review," in *Proc. Int. Conf. Elect. Mach.*, 2014, pp. 544–550.

[4] N. W. Frank and H. A. Toliyat, "Gearing ratios of a magnetic gear for wind turbines," in *Proc. IEEE Int. Elect. Mach. and Drives Conf.*, 2009, pp. 1224–1230.

[5] K. K. Uppalapati, J. Z. Bird, D. Jia, J. Garner, and A. Zhou, "Performance of a magnetic gear using ferrite magnets for low speed ocean power generation," in *Proc. IEEE Energy Convers. Congr. and Expo.*, 2012, pp. 3348–3355.

[6] M. Johnson, M. C. Gardner, H. A. Toliyat, S. Englebretson, W. Ouyang, and C. Tschida, "Design, Construction, and Analysis of a Large Scale Inner Stator Radial Flux Magnetically Geared Generator for Wave Energy Conversion," *IEEE Trans. Ind. Appl.*, vol. 54, no. 4, pp. 3305-3314, July/Aug 2018.

[7] L. MacNeil, B. Claus, and R. Bachmayer, "Design and evaluation of a magnetically-geared underwater propulsion system for autonomous underwater and surface craft," in *Proc. Int. Conf. IEEE Oceans*, 2014, pp. 1-8.

[8] T. V. Frandsen, L. Mathe, N. I. Berg, R. K. Holm, T. N. Matzen, P. O. Rasmussen, and K. K. Jensen, "Motor integrated permanent magnet gear in a battery electrical vehicle," *IEEE Trans. Ind. Appl.*, vol. 51, no. 2, pp. 1516–1525, Mar./Apr. 2015.

[9] J. J. Scheidler, V. M. Asnani and T. F. Tallerico, "NASA's Magnetic Gearing Research for Electrified Aircraft Propulsion," in *Proc. AIAA/IEEE Elect. Aircraft Technol. Symp.*, 2018, pp. 1-12.

[10] S. Pakdelian, M. Moosavi, H. A. Hussain, and H. A. Toliyat, "Control of an Electric Machine Integrated With the Trans-Rotary Magnetic Gear in a Motor Drive Train," *IEEE Trans. Ind. Appl.*, vol. 53, no. 1, pp. 106–114, Jan./Feb. 2017.

[11] M. Desvaux, R. Le Goff Latimier, B. Multon, S. Sire, and H. Ben Ahmed, "Analysis of the Dynamic Behaviour of Magnetic Gear with Nonlinear Modelling for Large Wind Turbines," in *Proc. Int. Conf. Elect. Mach.*, 2016, pp. 1332–1138.

[12] R. G. Montague, C. M. Bingham, and K. Atallah, "Magnetic Gear Dynamics for Servo Control," in *Proc. IEEE Mediterranean Electrotechnical Conf.*, 2010, pp. 1192–1197.

[13] M. Bouheraoua, J. Wang, and K. Atallah, "A Complex Frequency Domain Analysis of a Closed Loop Controlled Pseudo Direct Drive," in *Proc. Int. Conf. Elect. Mach.*, 2012, pp. 2428–2434.

[14] R. G. Montague, C. M. Bingham, and K. Atallah, "Dual-observer-based position-servo control of a magnetic gear," *IET Elect. Power. Appl.*, vol. 5, no. 9, pp. 708–714, Nov. 2011.

[15] M. C. Gardner, M. Johnson, and H. A. Toliyat, "Analysis of High Gear Ratio Capabilities for Single-Stage, Series Multistage, and Compound Differential Coaxial Magnetic Gears," *IEEE Trans. Energy Convers.*, vol. pp, no. 99, pp. 1-8, 2018.